processes

MDPI

Article

Modelling the Mechanism of Sulphur Evolution in the Coal Combustion Process: The Effect of Sulphur–Nitrogen Interactions and Excess Air Coefficients

Yu Jiang, Xinyu Yang and Honghe Ma *

School of Electrical and Power Engineering, Taiyuan University of Technology, Taiyuan 030024, China
* Correspondence: mahonghe@tyut.edu.cn

Abstract: The efficient use of coal resources and the safe operation of coal-fired boilers are hindered by high-temperature corrosion caused by corrosive sulphur components. To predict the impact of sulphur–nitrogen interactions on sulphur's evolution and its mechanism of action, a conventional sulphur component evolution model (uS–N) and an improved sulphur component evolution model (S–N) that considers sulphur–nitrogen interactions were proposed in the present study. The models were built using OpenFOAM–v8 software for the coal combustion process, and the generation of SO_2, H_2S, COS, and CS_2 was simulated and analysed under different air excess coefficients. The simulations were conducted to analyse the patterns of SO_2, H_2S, COS, and CS_2 generation at different air excess factors. The results show that, compared with the uS–N condition, the simulated values of coal combustion products (SO_2, H_2S, COS, and CS_2) under the S–N condition were closer to the experimental values, and the errors of different sulphur components at the furnace exit were all less than 5%. As such, the S–N model can more accurately predict the evolution of sulphur components. In the simulation range, when the air excess factor increased from 0.7 to 0.9, the production rate of SO_2 increased, while the production rates of corrosive sulphur components H_2S, COS, and CS_2 decreased significantly by 41.3%, 34.8%, and 53.8%, respectively. Further, the mechanism of the effect of sulphur–nitrogen interactions on the generation rates of different components was revealed at different air excess coefficients. Here, the effect of sulphur–nitrogen interactions on SO_2 and COS was found to be more significant at smaller air excess coefficients, and the effect of sulphur–nitrogen interactions on H_2S and CS_2 was more significant at larger air excess coefficients. The present study can provide a theoretical basis for predicting the evolution of sulphur components during coal combustion and improving the high-temperature corrosion problems caused by such a process.

Keywords: coal combustion; numerical simulation; high-temperature corrosion; sulphur evolution; sulphur–nitrogen interactions

Citation: Jiang, Y.; Yang, X.; Ma, H. Modelling the Mechanism of Sulphur Evolution in the Coal Combustion Process: The Effect of Sulphur–Nitrogen Interactions and Excess Air Coefficients. *Processes* **2023**, *11*, 1518. https://doi.org/10.3390/pr11051518

Academic Editor: Wei Li

Received: 13 April 2023
Revised: 12 May 2023
Accepted: 15 May 2023
Published: 16 May 2023

1. Introduction

Although there is widespread interest in exploring new energy sources, coal remains the primary source of energy globally. Coal accounts for more than 50% of China's energy structure, and thermal power units undertake the main power generation task for China's electricity demand. In China, clean coal combustion continues to be a significant factor in the energy supply. As demonstrated in the existing research, the implementation of air-graded combustion technology generates a strong reducing atmosphere in specific regions of the furnace. The reducing zone, created by air-graded combustion technology, is where corrosive sulphur-containing gases, such as H_2S and COS, tend to form at high levels [1]. The presence of corrosive sulphur-containing gases can easily lead to high-temperature corrosion of the water-cooled wall in the furnace chamber [2], which considerably affects the safe and stable operation of a boiler.

To mitigate the incidence of sulphide-induced high-temperature corrosion, the source of sulphide generation needs to be identified. Hence, understanding the evolution of the sulphur component during coal combustion under fuel-rich conditions is crucial. There have been numerous studies on the mechanism of sulphur fraction evolution. Maffei et al. [3] revealed a kinetic model for the pyrolysis of sulphur-containing components in coal through numerical simulation research, which integrates and improves the sulphur-containing component pyrolysis model established by Sugawara et al. [4] and Chen et al. [5]. In this model, organic sulphur and inorganic sulphur in coal powder are treated separately, and different pyrolysis models are established. The model can accurately predict the pyrolysis of SO_2 and H_2S. Ströhle et al. [6] proposed a gas-phase reaction mechanism model of sulphur-containing components through numerical simulation to study the reaction kinetics of SO_2 and H_2S components during coal combustion. The numerical simulation results showed that, as the coal combustion process progressed, the H_2S released during the devolatilisation process was rapidly oxidised and regenerated under reducing conditions. Under fuel-rich conditions, SO_2 reacts in the gas phase to form SO and H_2S. Maximilian Von Bohnstein et al. [7] used ANSYS Fluent software to simulate the process of coal combustion, incorporating gas-phase reaction mechanisms related to sulphides and chlorides to predict the generation of corrosive sulphides and chlorides, with a focus on observing the formation and evolution of SO_2, H_2S, COS, and HCl during coal combustion. The model can predict the evolution of corrosive sulphides and chlorides in coal-fired boilers.

However, the study found that the interaction between sulphur and nitrogen has a great influence on the evolution of sulphur components in the coal combustion process, and the study of the effect of sulphur–nitrogen interactions on the evolution of sulphur components has an important supplementary significance for the prevention and control of high-temperature corrosion. Chagger et al. [8] identified that during the combustion of CH_4, SO_2 causes a decrease in the concentration of NO_X and a small amount of H_2S is produced. Chagger et al. [9] later conducted further research on the primary reactions involved in the sulphur–nitrogen interactions and determined that the dominant reaction during fuel-rich conditions is HS + NO = SN + OH. Through both experiments and numerical simulations, Choudhury et al. [10] explored the interaction between sulphur and nitrogen components during combustion, respectively. Oxyfuel combustion experiments were performed using CH_4 gas doped with NO and SO_2 as fuel, and the addition of NO was found to lead to a decrease in the concentration of SO_3. The interaction between SO_2 and NO during methane combustion was investigated by Wang et al. [11]. Using Chemkin software, the addition of SO_2 under fuel-rich conditions promoted the production of NO, and the key radical reactions were NH + SO = NO + SH and SO_2 + H = SO + OH. Subsequently, Wang et al. [12] investigated the synergistic promotion of SO_X and NO_X. Findings were made that SO_X and NO_X could improve the conversion of SO_2 through an interaction between SO_X and NO_X. Through simulations, Xiao et al. [13] showed that the reduction of NO was promoted by sulphur-containing substances under oxygen-poor conditions, and that SH and SN radicals could directly reduce NO. Kang et al. [14] investigated the effect of NO on H_2S production and found that NO would inhibit the production of H_2S. At present, sulphur and nitrogen interactions are commonly investigated by introducing sulphur- and nitrogen-containing components to establish the relevant experimental conditions. However, such an approach may not entirely elucidate the mechanism underlying the influence of sulphur–nitrogen interactions on the evolution of sulphur during coal combustion.

In the present study, in order to better predict the influence of sulphur–nitrogen interactions on sulphur evolution and the mechanism of action in fuel-rich operating conditions, a conventional sulphur component evolution model (uS–N) and an improved sulphur component evolution model (S–N) considering sulphur–nitrogen interactions were developed for the coal combustion process. OpenFOAM–v8 software was used to investigate the generation of SO_2, H_2S, COS, and CS_2 under different air excess coefficients.

2. Simulation Methodology

2.1. Coal Combustion Model

The whole simulation process was conducted in OpenFOAM–v8. Such process involved the movement of coal particles, the flow and heat exchange between the two phases, the pyrolysis of coal, the combustion of coke, the gas-phase reaction, and other processes, which required the development of relevant calculation models. The Euler–Lagrange model was used for the calculation of the gas–solid two-phase flow, the motion of the particles was simulated using the DPM model, turbulence was calculated via the Reynolds time-averaged model, the interaction between chemical reactions and turbulence was selected from the finite rate/vortex dissipation model, the P-1 model was used to deal with radiative heat transfer, and the PASR model was used for the combustion model.

The coal combustion process was simulated under conditions of fuel-richness, which would result in incomplete combustion of the coal. To account for such conditions, the gasification and oxidation reactions of coke needed to be considered, as well as the pyrolysis model of sulphur and nitrogen components [7,15] and relevant gas-phase reaction models [16,17].

Nitrogen in coal mainly exists in the form of nitrogen-containing organic compounds. A portion of the nitrogen in nitrogenous organic compounds releases as volatile fraction nitrogen to produce nitrogenous substances such as HCN and NH_3. The remaining nitrogen is still present in the coke in the form of nitrogen-containing organic matter. In the subsequent combustion process, the nitrogen in the coke will also produce nitrogen-containing substances such as HCN and NH_3 [16]. Nitrogen-containing components such as HCN and NH_3 oxidise with oxygen to form nitrogen oxides, while they also reduce the generated nitrogen oxides to N_2. Relevant studies have shown that NO accounts for more than 90% of the total nitrogen oxides [18]. Therefore, the main nitrogen oxide selected in this paper is NO. The gas-phase reaction mechanism of the nitrogen components is presented in Table 1 [17,19].

Table 1. Gas-phase reaction model of nitrogen components.

Reaction	A	E/(cal/mol)
$4NH_3 + 5O_2 = 4NO + 6H_2O$	4×10^6	31,989
$4HCN + 7O_2 = 4NO + 4CO_2 + 2H_2O$	1×10^{10}	66,964
$4NH_3 + 6NO = 5N_2 + 6H_2O$	1.8×10^8	27,067
$4HCN + 10NO = 7N_2 + 4CO_2 + 2H_2O$	3×10^{12}	59,964
$NO + CO = 1/2N_2 + CO_2$	1×10^{14}	79
$NO + H_2 = 1/2N_2 + H_2O$	1×10^{11}	79
$HCN + O = NCO + H$	1.4×10^4	20,836
$NCO + H = NH + CO$	7.2×10^{13}	4184
$NH_3 + O = NH_2 + OH$	9.4×10^6	27,029
$NH_2 + H = NH + H_2$	4×10^{13}	15,272
$NH_2 + OH = NH + H_2O$	4×10^6	4184
$NH_2 + O = NH + OH$	6.8×10^{12}	0
$NH + O_2 = NO + OH$	1.3×10^6	418
$NH + O = NO + H$	9.2×10^{13}	0

Elemental sulphur occurs in coal in both inorganic and organic forms. Organic sulphur mainly includes fatty sulphur, thiophene sulphur, and aromatic sulphur, while inorganic sulphur mainly exists in the form of pyrite sulphur and sulphate sulphur [20]. In coal pyrolysis, the release process of organic sulphur involves a wide variety of intermediate reactions and intermediate products. As a result, it is difficult to reproduce the complete organic sulphur pyrolysis process using OpenFOAM–v8 [21,22]. Therefore, this paper employs simplified modelling of the release and transformation process of organic sulphur in coal combustion using four distinct pyrolysis products: SO_2, H_2S, COS, and CS_2 [23]. Since the inorganic sulphur in coal mainly contains pyrite sulphur and sulphate sulphur,

while the selected coal species has a very low sulphate sulphur content, inorganic sulphur is represented by calcium sulphate in the numerical simulations [7].

There are three principal models for the gas-phase reaction mechanism of sulphur components: the lumped reaction model, the detailed reaction model, and the simplified reaction model. The lumped reaction model does not consider the gas-phase reaction of sulphur components from the free base plane. The detailed reaction model contains a large number of reactions, so the numerical simulation of the combustion chamber has conflicting accuracy and poor computational efficiency. However, the simplified model takes into consideration the gas-phase reactions of sulphur components from the free base level and accurately predicts their concentration distribution. As a result, it can be applied in engineering design to improve computational efficiency [24]. Therefore, the model for sulphur components used in this paper was the simplified reaction mechanism model.

In this paper, a conventional evolutionary gas-phase reaction mechanism model for sulphur components (uS–N) was constructed for performing numerical simulations [24,25]. The uS–N mechanism model includes reactions between sulphur components such as SO_2, H_2S, COS, and CS_2, sulphur-containing radicals including SH and SO, and active radicals O_2, CO_2, CO, H_2, H_2O, O, OH, and H. These reactions apply to low-NO_X and are suitable for fuel-rich combustion conditions under low-NO_X combustion conditions. The relevant reactions are listed in Table 2.

Table 2. Conventional evolutionary gas-phase reaction mechanism model for sulphur components.

Reaction	A	E/ (cal/mol)	Reaction	A	E/ (cal/mol)
$H_2S + M = S + H_2 + M$	1.6×10^{24}	44,800	$SO_2 + H = SO + OH$	7.69×10^{9}	28,357
$H_2S + H = SH + H_2$	1.2×10^{7}	350	$CO + SO = CO_2 + S$	5.1×10^{13}	53,400
$H_2S + O = SH + OH$	7.5×10^{7}	1460	$SO + OH = SO_2 + H$	1.08×10^{17}	0
$H_2S + OH = SH + H_2O$	2.7×10^{12}	0	$CS_2 + O = COS + S$	7.1×10^{12}	2102
$H_2S + S = SH + SH$	8.3×10^{13}	3700	$CS_2 + O = CS + SO$	3.6×10^{13}	1696
$S + H_2 = SH + H$	1.4×10^{14}	9700	$CS + O_2 = CO + SO$	6.1×10^{12}	16,500
$SH + O = H + SO$	1×10^{14}	0	$CS_2 + OH = COS + SH$	5.79×10^{8}	−1174
$SH + OH = S+H_2O$	1×10^{13}	0	$COS + OH = CO_2 + SH$	7.9×10^{8}	0
$SH + O = S + OH$	6.3×10^{11}	4030.6	$CS_2 + H_2O = H_2S + COS$	1.74×10^{11}	41,497
$S + OH = H + SO$	4×10^{13}	0	$COS + H_2O = H_2S + CO_2$	1.71×10^{10}	35,299
$HOSHO = H + SO_2$	1.95×10^{10}	46,933	$CO + SH = COS + H$	2.87×10^{7}	15,200
$SO + M = S + O+M$	4×10^{14}	54,000	$COS + M = CO + S+M$	6.88×10^{6}	30,700
$SO + OH = HOSO$	1.6×10^{12}	−400	$SO_2 + 3CO = COS + 2CO_2$	8.6×10^{12}	87,700
$SO + O = SO_2$	3.2×10^{13}	0	$O + COS = CO + SO$	1.93×10^{13}	2328.6
$2SO = SO_2 + S$	2×10^{12}	2000	$O + COS = CO_2 + S$	5×10^{13}	5530.4
$SO_2 + CO = SO + CO_2$	2.7×10^{12}	24,300			

To reflect the influence of sulphur–nitrogen interactions on the evolution of the sulphur fraction, four radical reactions involving the radicals SH, SO, NH, NO, and SN were added to the previous gas-phase reaction model. The reactions together formed an improved model for the evolution of the sulphur fraction (S–N) considering sulphur–nitrogen interactions. The radical reactions associated with sulphur–nitrogen interactions are shown in Table 3 [13,24–26].

Table 3. Main reactions involved in the uS–N model and S–N model.

Reaction	A	E/(cal/mol)	Ref.	uS–N	S–N
SO + NH = NO + SH	3.01×10^{13}	0	[26]	-	√
SH + NO = SN + OH	1×10^{13}	8900.6	[26]	-	√
SN + NO = N_2 + SO	1.81×10^{10}	0	[26]	-	√
SH + NO = NH + SO	1×10^{9}	0	[13]	-	√
SO_2 + H = SO + OH	7.691×10^{9}	28,357	[26]	√	√
SO_2 + CO = SO + CO_2	2.7×10^{12}	24,300	[25]	√	√
H_2S + H = SH + H_2	1.2×10^{7}	350	[25]	√	√
H_2S + O = SH + OH	7.5×10^{7}	1460	[25]	√	√
H_2S + OH = SH + H_2O	2.7×10^{12}	0	[25]	√	√
H_2S + S = SH + SH	8.3×10^{13}	3700	[25]	√	√
CO + SH = COS + H	2.87×10^{7}	15,200	[25]	√	√
COS + OH = CO_2 + SH	7.9×10^{8}	0	[25]	√	√
CS_2 + O = CS + SO	3.6×10^{13}	1696	[25]	√	√
CS + O_2 = CO + SO	6.1×10^{12}	16,500	[25]	√	√
CS_2 + OH = COS + SH	5.79×10^{8}	−1174	[25]	√	√

√ The reactions included in the model; - The reactions not included in the model.

2.2. Physical Model and Boundary Conditions

The object of the present study was an 18 kW DC coal burner. The physical structure and meshing of the burner are shown in Figure 1. The main body of the burner chamber is cylindrical, with an inner diameter of 0.15 m and a length of 2.2 m. The primary and secondary air channels are located at the top, with an inner diameter of 8 mm for the primary air channel and a width of 14 mm for the secondary air channel, which is an annular channel outside the primary air channel. In order to verify the mesh irrelevance, simulations were conducted for combustor models with mesh numbers 130,799, 73,515, and 35,013, respectively. The temperature variation in the central axis of the furnace was basically the same for grid numbers 130,799 and 73,515 and differed more significantly from that for grid number 35,013. As such, the model with grid number 73,515 was chosen.

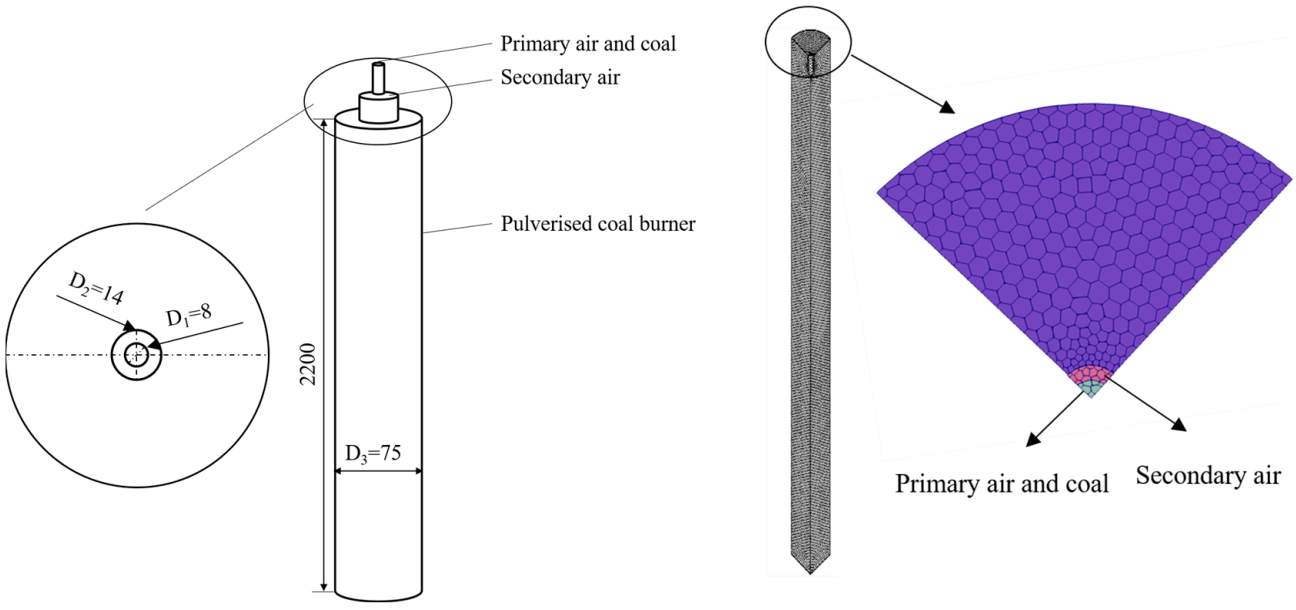

(**a**) Burner structure (**b**) Grid

Figure 1. Burner structure and grid.

The coal used was Daheng coal, and the coal properties are shown in Table 4. The primary air temperature was 353 K, the secondary air temperature was 623 K, and the air-fuel ratio was maintained at 0.8. Other combustion conditions are shown in Table 5.

Table 4. Coal properties.

Proximate Analysis/%				Elemental Analysis/%				
M_{ar}	V_{ar}	FC_{ar}	A_{ar}	C_{daf}	H_{daf}	O_{daf}	N_{daf}	S_{daf}
9.60	24.14	35.41	30.84	78.08	5.65	13.87	1.82	0.56

Table 5. Combustion conditions.

Parameter	Value
Mass flow of pulverised coal (kg/h)	0.45
Primary air velocity (m/s)	6.315
Secondary air velocity (m/s)	5.457
Primary air temperature (K)	353
Secondary air temperature (K)	623
Excess air coefficient	0.8
Environment pressure (Pa)	91,920

To analyse the evolution of sulphur components under different fuel-rich conditions, three different excess air coefficients were set, as shown in Table 6. Numerical simulations of the pulverised coal combustion process with different excess air coefficients were performed to analyse the concentration distribution of each component at different excess air coefficients and to investigate the effect of excess air coefficients on the evolution of sulphur components under fuel-rich conditions. Under varying excess air coefficients, the wind speed of primary air remained constant, while only the wind speed of secondary air was adjusted. This is because the wind speed of primary air was established based on the design parameters of the DC coal burner. The quality flow of primary air was 2.2 times that of coal quality flow.

Table 6. Fuel and air intake settings under different operating conditions.

Excess Air Coefficient	Mass Flow of Pulverised Coal (kg/h)	Primary Air Velocity (m/s)	Secondary Air Velocity (m/s)
0.7	0.45	6.315	4.278
0.8	0.45	6.315	5.457
0.9	0.45	6.315	6.636

3. Results and Discussion

3.1. Model Reliability Validation

Figure 2 presents a curve illustrating how the temperature changes in the central axis of the furnace chamber. It reveals that the temperature in the furnace rises slowly from the furnace inlet to the axial distance of 350 mm. This area is mainly heated by pulverised coal and fresh air brought in by the primary and secondary air inlets in the furnace. Between an axial distance of 350 mm and 500 mm, the temperature climbs sharply at the centre line of the furnace chamber and the temperature gradient changes significantly. The combustion reaction primarily occurs in this region, where the volatile fraction and the coke burn quickly to release a large amount of heat. The highest temperature occurs near Z = 500 mm with a peak of 1504 K. After the combustion reaction is complete, the temperature drops rapidly to approximately 1050 K. Subsequently, the variation in temperature decreases and the temperature drops slowly to around 1000 K. The homogeneous reaction between the gas phases mainly occurs in the reduction zone, which is downstream of the furnace chamber. Therefore, the reaction heat release is low, and the temperature change is small.

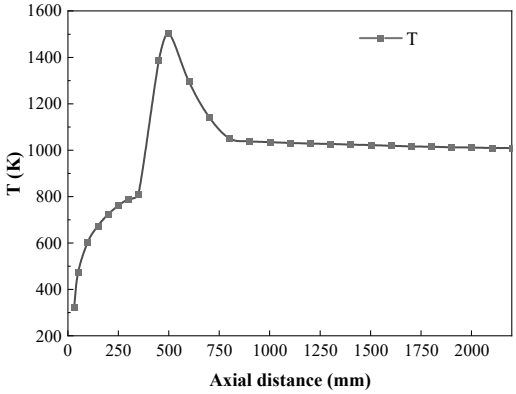

Figure 2. Temperature variation curve on the central axis of the furnace.

To verify the reliability of the numerical simulation method, the simulation results were compared with the experimental data from prior research [23]. A comparison of the simulated and experimental values of the concentrations of the main gas components is shown in Figure 3. In Figure 3, an observation can be made that the average error between the simulated and experimental values of the concentrations of O_2, CO_2, CO, and H_2 was within 10%, and the error at the furnace exit was within 5%. Such results indicate that the simulation methods can accurately predict the coal combustion process and that the model can be used to predict the evolution of sulphur components.

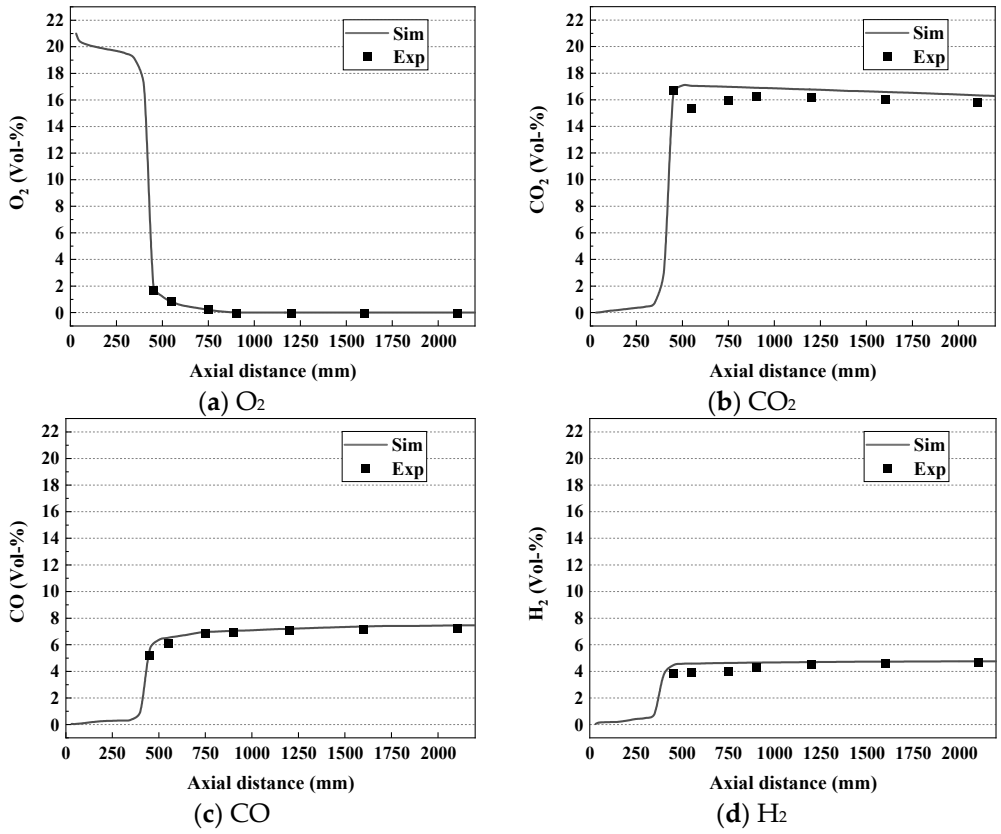

Figure 3. Comparison between the simulation and the experiment of the main gas components on the central axis of the furnace.

3.2. Comparison of the Sulphur Evolution during Coal Combustion under uS–N and S–N Conditions

Figure 4 reveals how the concentration of NO varies on the centre line of the furnace chamber under uS-N and S-N conditions. It also shows a comparison with the experi-

mental values. The figure indicates that the trend of the changing concentration for NO on the central axis is very similar under both operating conditions. Initially, the NO concentration increases due to pyrolysis of the nitrogen-containing material in the coal. As the temperature increases in the main combustion zone, the oxidation reaction rate of the nitrogen-containing components, such as HCN and NH_3, to produce NO increases, leading to a rapid rise in the NO concentration. Next, as the O_2 concentration falls, the furnace atmosphere transforms into a reducing atmosphere and the reduction of NO by reducing gases leads to a decrease in the concentration of NO. By comparing the average error between the simulated and experimental NO values under the two conditions, the average error under S–N conditions is 2.5% and 3.7% under uS-N conditions. This indicates that the model can accurately simulate the formation of NO_X.

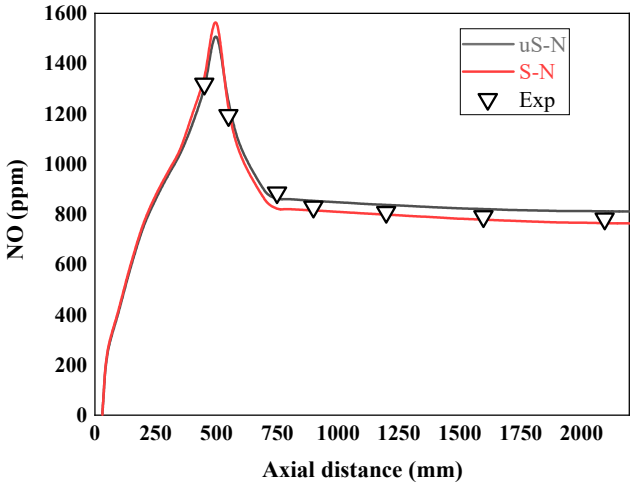

Figure 4. The variation of NO concentration on the centre axis of the furnace chamber for uS–N and S–N (excess air factor 0.8).

Figure 5 displays the concentration profiles of the sulphur components on the centre line of the furnace chamber under both the uS–N and S–N conditions. The results indicate that varying temperatures affect changes in the evolution of the sulphur components [7]. The trends regarding the sulphur fraction concentration along the central axis are remarkably similar for both conditions. Initially, the concentrations of SO_2, H_2S, COS, and CS_2 increase due to the pyrolysis of the sulphur-containing material in the pulverised coal. As the temperature increases in the main combustion zone, the reaction rate of H_2S, COS, and CS_2 reacting with O_2 to generate SO_2 increases, and the concentration of SO_2 rapidly increases. Afterwards, the atmosphere inside the furnace changes to a reducing atmosphere as the O_2 concentration decreases. The reduction of SO_2 by reducing gases leads to a decrease in the concentration of SO_2 and promotes the generation of H_2S and COS. The concentration of H_2S and COS increases. The reaction of CS_2 with H_2O resulted in a decrease in the concentration of CS_2 in the furnace chamber.

Comparing the average error between the simulated and experimental values under uS–N and S–N conditions, the average error of SO_2 under S–N conditions was 3.2%, which was lower than 8.2% under uS–N conditions; the average error of H_2S under S–N conditions was 13.5%, which was lower than 17.2% under uS–N; and the average error of COS under S–N conditions and uS–N conditions was 6.0%. The mean error of CS_2 was 16.0% under S–N conditions, which was slightly higher than the mean error of 14.5% under uS-N conditions. As Figure 5d reveals, there is a local deviation between the simulated and experimental values of CS_2 in the high-temperature region of the reduction zone in the furnace chamber. A possible explanation for this phenomenon is that the generated CS_2 in the experiment is unevenly distributed in the furnace chamber and there is a certain error in the instrumental measurements of the experimental values. Additionally, the reactions in which CS_2 is involved in this region are very complex. For instance, Clark et al. [27] and

Abián et al. [28] showed that CS_2 reacts with a variety of substances such as H_2O, CO_2, SO_2, SO, H_2, etc., in the high-temperature region of the reduction zone. The reaction mechanism here has not yet been determined, and simulations cannot fully reflect how the reaction proceeds. However, the average error between the simulated values and the experimental values of the models used for both S–N and uS–N conditions is generally around 15.2%. Therefore, more detailed experimental studies regarding CS_2 should be conducted in the future. The mean error of CS_2 was 16.0% in S–N, which was slightly higher than the mean error of 14.5% in uS–N. Comparing the errors between the simulated and experimental values at the furnace exit for uS–N and S–N conditions, the errors were 1.8% for SO_2, 2.8% for H_2S, 3.0% for COS, and 4.1% for CS_2 for the S–N conditions, and 7.3% for SO_2, 6.3% for H_2S, 9.0% for COS, and 12.2% for CS_2 for the uS–N conditions. The error of CS_2 was 12.2%. An observation can be made that the prediction results of SO_2, H_2S, COS, and CS_2 for the S–N condition were significantly better than those for the uS–N condition, thus indicating that the numerical model improved the accuracy of the prediction of the evolution of the sulphur components after considering sulphur–nitrogen interactions.

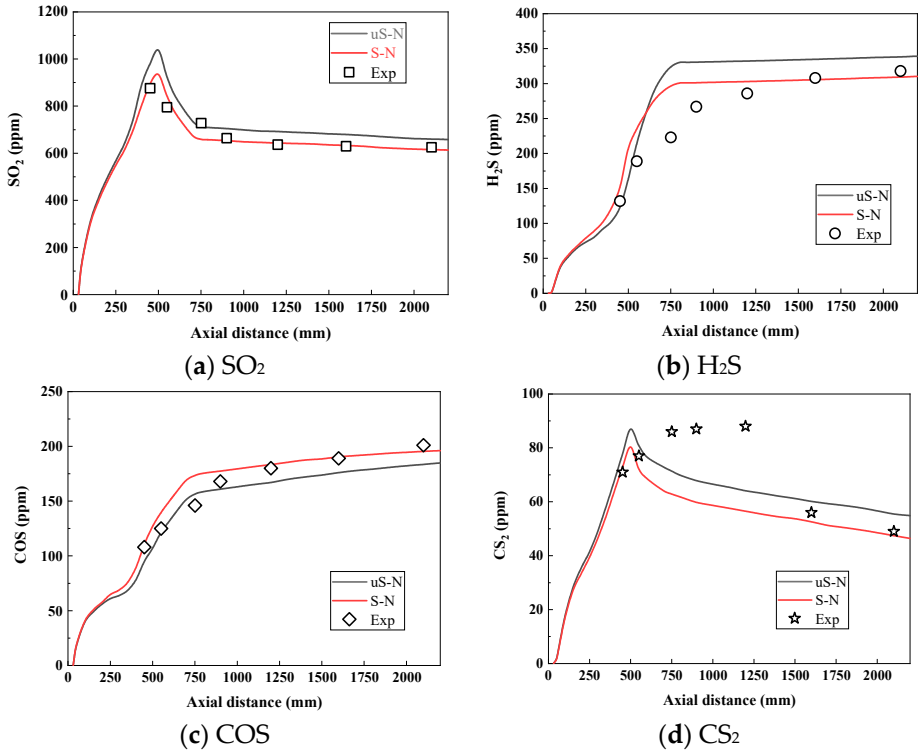

Figure 5. The variation of sulphur concentration on the centre axis of the furnace chamber for uS–N and S–N (Excess air factor 0.8).

When comparing the concentration profiles of the sulphur components in the uS–N and S–N conditions, the SO_2 concentration in the uS–N condition was higher than that in S–N condition; the H_2S concentration in the S–N condition was higher in the main combustion zone than that in the disregarded condition, and after entering the reduction zone, the H_2S concentration in the uS–N condition increased rapidly and exceeded that in the S-N condition; the COS concentration in the main combustion zone was higher than that in the uS–N condition, and after entering the reduction zone, the increase in the COS concentration value in the considered condition was smaller than that in the unconsidered condition, and the difference in COS concentration values between the two conditions decreased; and the CS_2 concentration in the S–N condition was lower than that in the uS–N condition. The reasons for such findings were as follows: (1) In the main combustion zone, the sulphur–nitrogen interactions were manifested by the consumption of SO radicals through the reaction SO + NH = NO + SH to produce SH radicals, which could be generated

through the consumption of SO_2 and CS_2, while the increase in SH radicals would promote the generation of H_2S and COS. (2) In the reduction zone, sulphur and nitrogen interactions were mainly reflected in the reduction of NO by SH radicals and SN radicals, and the reactions occurred as SH + NO = SN + OH, SN + NO = N_2 + SO, and SH + NO = NH + SO. Such a process consumed SH radicals and generated SO radicals. The presence of radicals led to an increase in their concentration, which could inhibit the reduction of SO_2.

3.3. Influence of Different Excess Air Coefficients on the Sulphur Evolution during Coal Combustion

The excess air ratio has a substantial effect on the temperature in the combustion chamber. Figure 6 compares the temperature curves for different excess air ratios and reveals that the average temperature on the centre line of the furnace chamber increases with rising excess air ratios. The excess air ratio affects the temperature in the combustion chamber because more oxygen is entering the chamber. Accordingly, more oxygen reacts with the coal, thereby increasing the temperature.

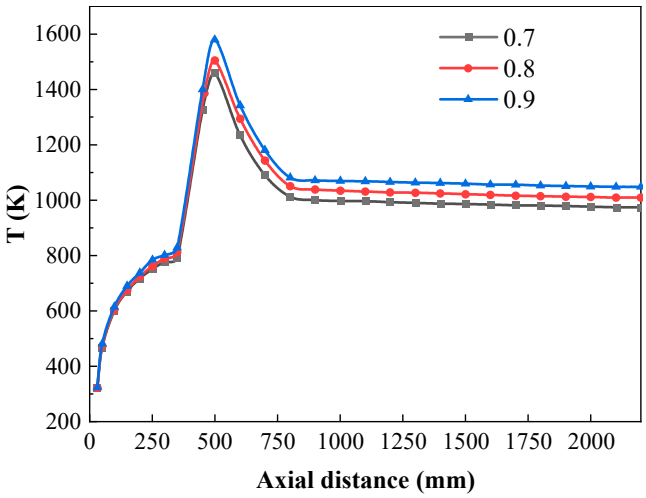

Figure 6. Temperature variation curve on the central axis of the furnace with different air excess coefficients.

Figure 7 indicates how the concentrations of O_2, CO_2, CO, and H_2 vary for different excess air coefficients on the central axis of the furnace chamber. According to Figure 7a, the simulated values of the O_2 volume fractions follow the same trend for different excess air coefficients. The O_2 concentration decreases slowly as the primary and secondary air enters the furnace chamber. After the volatile fraction and the coke start to burn, the O_2 concentration drops sharply. Under fuel-rich conditions, the O_2 is almost completely consumed after the combustion reaction. As Figure 7b,c shows, the CO_2 volume fraction rises with an increasing excess air factor, while the CO volume fraction drops as the excess air factor increases. This is because the amount of oxygen entering the furnace chamber grows as the excess air factor increases. Additionally, coal burns better under conditions with a higher air excess coefficient, so more CO_2 is produced through complete combustion of the coke with oxygen and less CO is produced by incomplete combustion. Moreover, the amount of residual char present in the reduction zone falls, thereby reducing the amount of CO produced by the reduction reaction. Finally, Figure 7d reveals that the H_2 volume fraction drops with increasing excess air. This is due to an increase in the amount of oxygen entering the furnace chamber, resulting in more H_2 being consumed in the main combustion zone. Thus, as the amount of oxygen entering the furnace chamber increases, the amount of residual H_2 falls and less H_2 is produced. At the same time, the amount of residual carbon present in the reduction zone decreases, thereby lowering the amount of H_2 produced from the reduction reaction between the residual carbon and H_2O in the reduction zone.

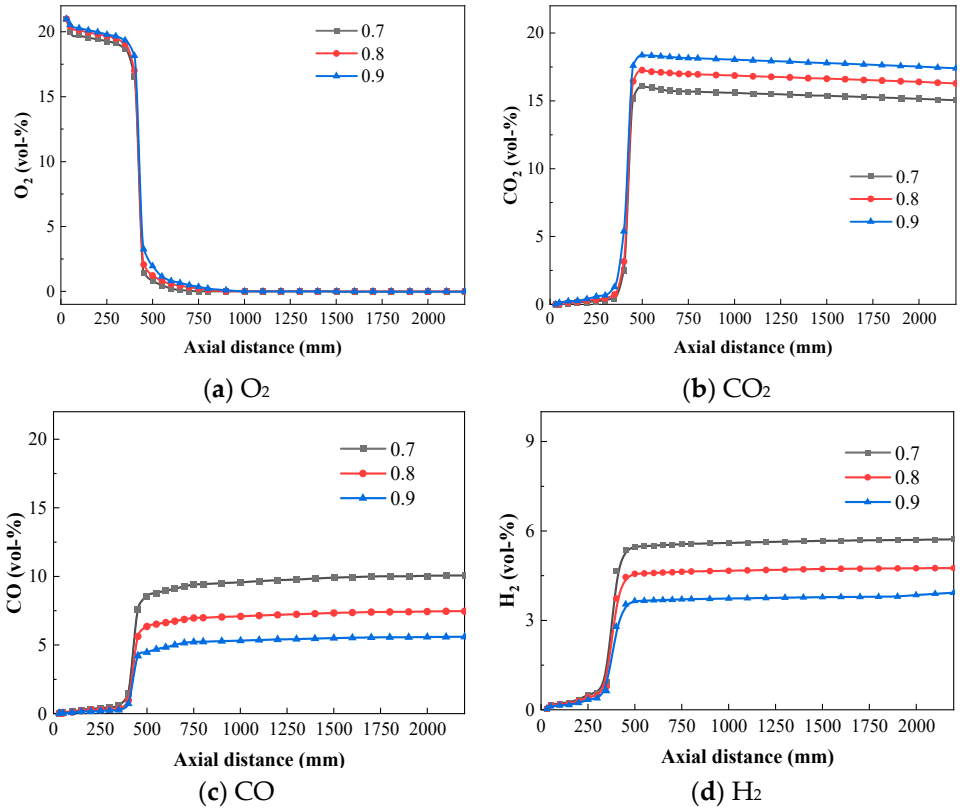

Figure 7. O_2, CO_2, CO, and H_2 on the central axis of the furnace with different air excess coefficients.

Regarding sulphur–nitrogen interactions, the simulation results for NO with different excess air coefficients are shown in Figure 8. The production rate of NO rises with an increasing excess air coefficient. Compared with the production rate at 0.7, the production rate increases by 24.0% at 0.8 and 48.6% at 0.9. The reason for this is that as the excess air coefficient increases, the amount of oxygen upstream of the furnace rises, and the temperature of the main combustion zone in the furnace climbs. Subsequently, the oxidation rate of NH_3, HCN, etc., increases, thereby promoting the production of NO. Downstream from the furnace, an increasing excess air coefficient leads to a drop in the concentration of the reducing gas. Additionally, the rate of the NO reduction reaction decreases, which moderates the reduction of NO.

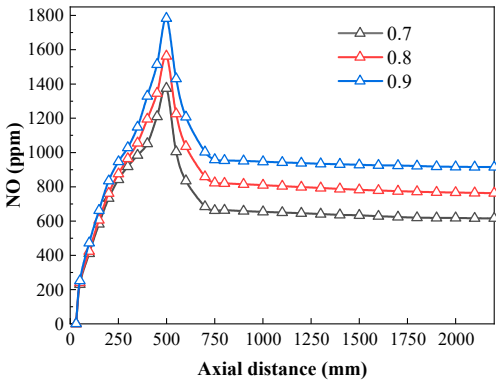

Figure 8. Effects of different excess air coefficients on NO in coal combustion.

The simulation results for the sulphur fraction with different excess air coefficients considering sulphur–nitrogen interactions are shown in Figure 9. An observation can be made that the production rate of SO_2 increased with increasing excess air coefficient, and compared with the production rate at 0.7, the production rate increased by 24.6% at 0.8

and 53.0% at 0.9; the production rates of H_2S, COS, and CS_2 decreased with an increasing excess air coefficient. The production rate of H_2S decreased by 19.3%, COS decreased by 18.7%, and CS_2 decreased by 33.3% at an excess air factor of 0.8, while the production rates of H_2S, COS, and CS_2 decreased by 41.8%, 34.9%, and 56.5%, respectively, at an excess air factor of 0.9. The reasons for such findings were as follows: At higher excess air coefficients, the amount of oxygen upstream of the furnace chamber rises and the temperature in the main combustion zone climbs. Consequently, the oxidation rates of H_2S, COS, and CS_2 increase, and the oxidation reaction consumes more H_2S, COS, and CS_2. Downstream from the furnace chamber, increased excess air coefficients lead to a decrease in the concentration of the reducing gas. As a result, the rate of the SO_2 reduction reaction decreases, and the amount of H_2S and COS generated by the SO_2 reduction falls. Moreover, CS_2 reacts with H_2O downstream from the chamber, leading to a decrease in the CS_2 concentration. The above analysis suggests that under fuel-rich conditions, increasing the excess air factor reduces the generation of the corrosive sulphur-containing gases, H_2S, COS, and CS_2.

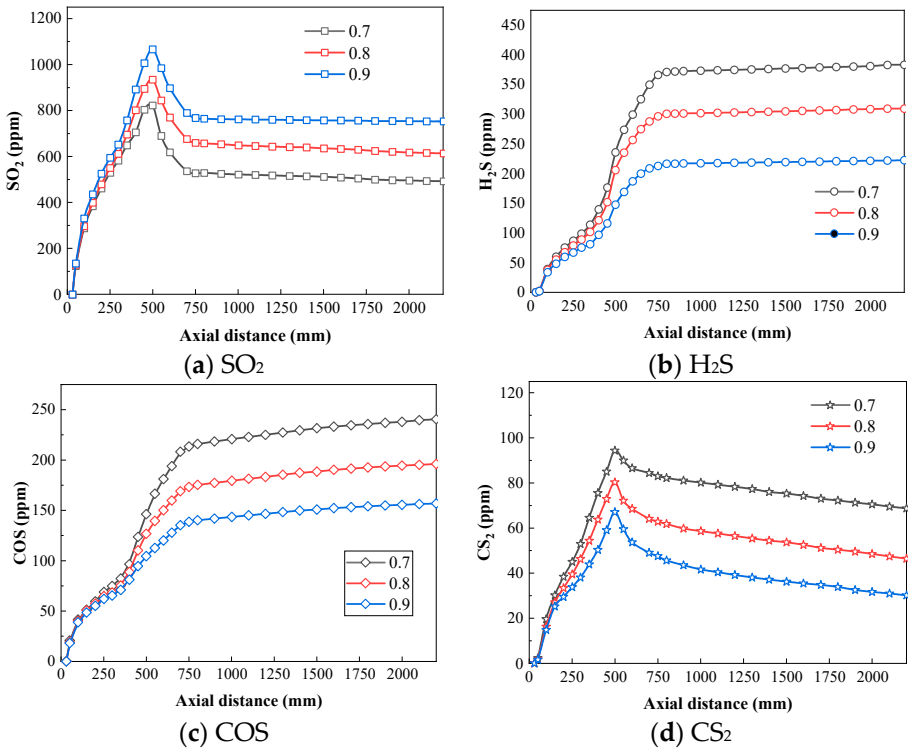

Figure 9. Effects of different excess air coefficients on the sulphur components in coal combustion.

As shown in Figure 10, the SO_2 concentration in the S–N condition was lower than that in the uS–N condition, and as the excess air coefficient increased, the difference between the concentration change curves of SO_2 in the S–N and uS–N conditions on the centreline of the furnace decreased. The difference between the SO_2 generation rate under S–N conditions and uS–N conditions was 13.4% for an excess air factor of 0.7, 6.8% for an excess air factor of 0.8, and 3.5% for an excess air factor of 0.9. The reasons for such results were as follows: (1) In the main combustion zone upstream of the furnace, the sulphur–nitrogen interactions mainly affected SO_2 generation through the reaction of SO + NH = NO + SH consuming SO. With the increase in the excess air coefficient, the amount of oxygen in the furnace increased and the NH radical was consumed more by oxygen, reducing the effect on SO_2 generation. Thus, the difference between the peak SO_2 concentration under S–N and uS–N conditions decreased with the increase in the excess air coefficient. (2) In the reduction zone, the sulphur–nitrogen interactions were mainly through the reactions of SH + NO = SN + OH, SN + NO = N_2 + SO, and SH + NO = NH + SO to produce SO radicals to suppress SO_2 consumption. With the increase in the excess air factor, the production of NO increased,

and more SO was produced in the reduction zone, which reduced the SO_2 consumption. As such, the difference in the SO_2 concentration at the furnace exit between S–N and uS–N conditions diminished with the increase in the excess air factor.

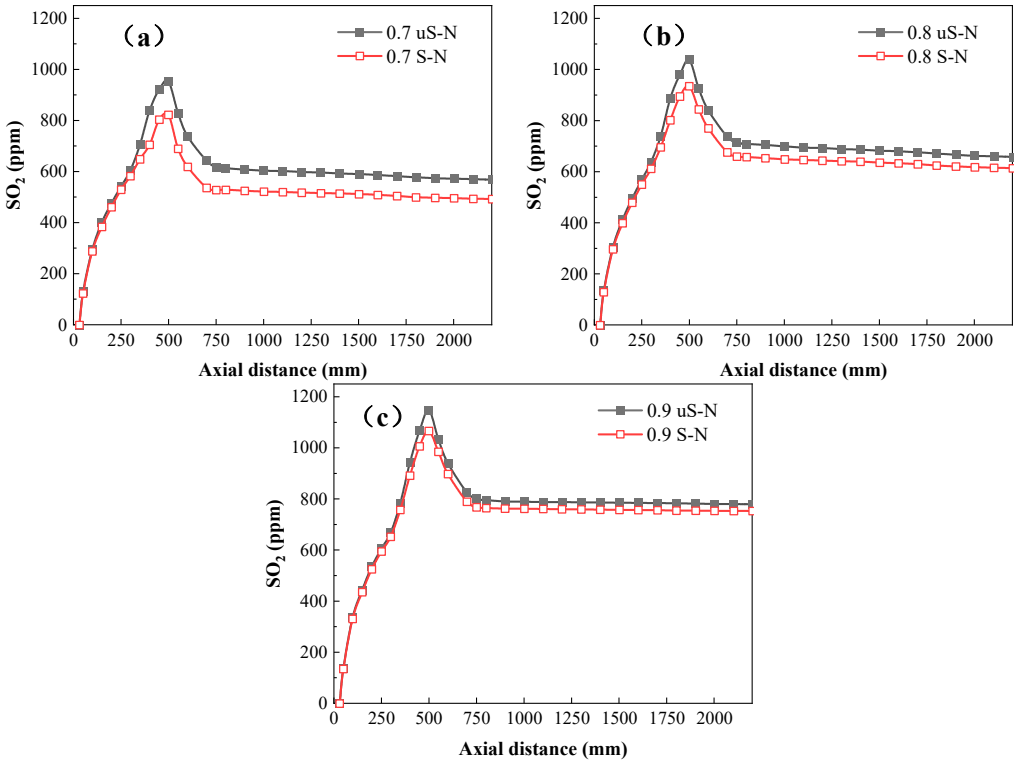

Figure 10. Effects of different excess air coefficients on SO_2 concentration on the central axis of the coal combustion chamber for uS–N and S–N: (**a**) 0.7; (**b**) 0.8; (**c**) 0.9.

As shown in Figure 11, the H_2S concentration values in the upper part of the furnace chamber in the S–N condition were greater than those in the uS–N condition, and the difference in H_2S concentration values decreased after entering the reduction zone. Subsequently, the concentration values in the uS–N condition were greater than those in the S–N condition. The difference between the generation rate of H_2S in the S–N condition and the uS-N condition was 3.0% for an excess air factor of 0.7, 8.8% for an excess air factor of 0.8, and 17.7% for an excess air factor of 0.9. The reasons for such results were as follows: (1) In the main combustion zone upstream of the furnace, the sulphur–nitrogen interactions were mainly through the reaction of SO + NH = NO + SH to produce SH radicals to promote the generation of H_2S. With the increase in the excess air coefficient, the amount of oxygen in the furnace increased, and NH radicals were consumed by more oxygen, reducing the impact on the generation of H_2S. Thus, the difference in H_2S concentration values between S-N and uS-N conditions decreased as the excess air coefficient increased and decreased. (2) In the reduction zone, the sulphur–nitrogen interactions were mainly through the reactions of SH + NO = SN + OH, SN + NO = N_2 + SO, and SH + NO = NH + SO consuming SH radicals to promote the consumption of H_2S. With the increase in the excess air coefficient, the concentration of NO increased, and the consumption of SH radicals in the reduction zone increased, which in turn increased the consumption of H_2S. Thus, the intersection point of the H_2S concentration values between S–N and uS–N conditions on the centreline of the furnace chamber was constantly advancing, while the contrast in the concentration values of H_2S between S–N and uS–N conditions at the furnace exit continued to grow. When the excess air factor is large, i.e., an excess air factor of 0.9 under rich fuel conditions, the analysis of the corrosive sulphur-containing H_2S gas should consider the sulphur–nitrogen interactions.

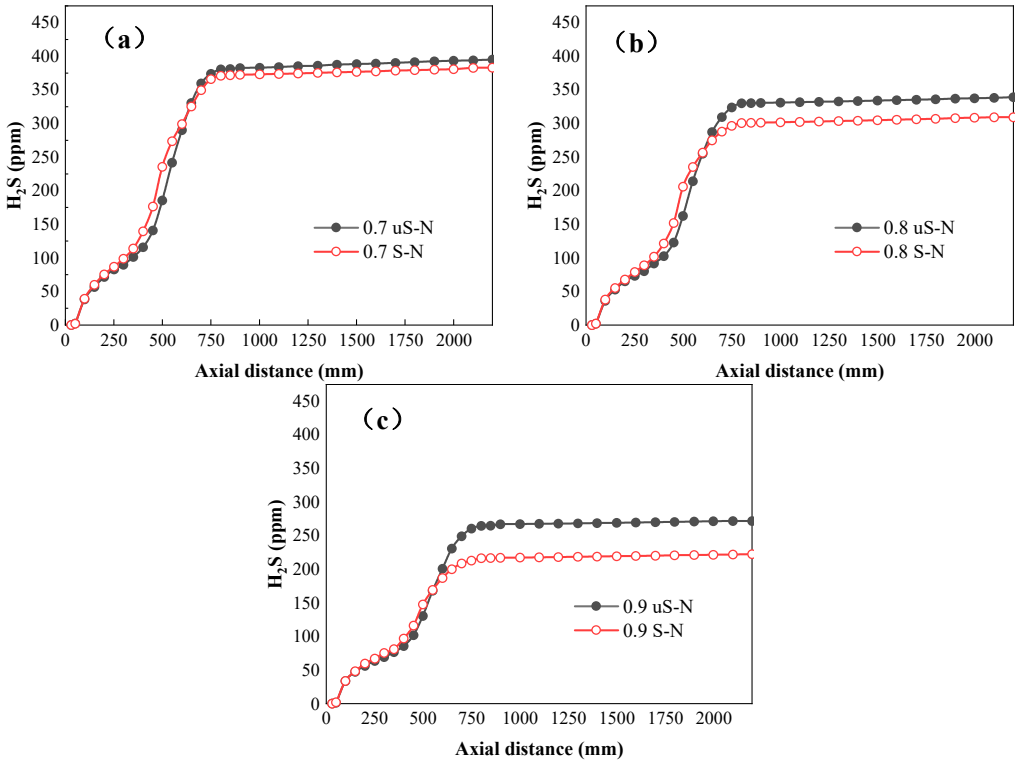

Figure 11. Effect of different excess air coefficients on H_2S concentration on the central axis of the coal combustion chamber for uS–N and S–N: (**a**) 0.7; (**b**) 0.8; (**c**) 0.9.

As shown in Figure 12, the COS concentration in the S–N condition was lower than that in the uS–N condition, and as the excess air factor increased, the difference between the concentration change curves of COS in the S–N and uS–N conditions on the centreline of the furnace decreased. The difference between the generation rate of COS in the S–N condition and the uS–N condition was 7.6% for an excess air factor of 0.7, 5.9% for an excess air factor of 0.8, and 4.0% for an excess air factor of 0.9. The reasons for such results were as follows: (1) In the main combustion area upstream of the furnace, COS could be generated through the reaction CO + SH = COS + H. The sulphur–nitrogen interactions primarily occurred through the reaction of SO + NH = NO + SH, resulting in the generation of SH radicals that facilitated the production of COS. However, with an increase in the excess air coefficient of oxygen in the furnace, NH radicals were more readily consumed by oxygen, leading to a decrease in the concentration of NH radicals. Such conditions, in turn, resulted in a reduction in the production of SH radicals and a subsequent decline in the promotion of COS generation. (2) In the reduction zone, the sulphur–nitrogen interactions mainly promoted COS consumption by consuming SH radicals, which could be generated through the reaction of COS + OH = CO_2 + SH. As the excess air factor increased, the amount of NO generated increased and the reduction of NO consumed more SH radicals, which promoted COS consumption. For the aforementioned reasons, the difference in the SO_2 concentrations at the furnace exit between S–N and uS–N conditions diminished with the increase in the excess air factor. When the excess air factor is small, i.e., 0.7 for fuel-rich conditions, the analysis of COS in the corrosive sulphur-containing gas should take into account the sulphur–nitrogen interactions.

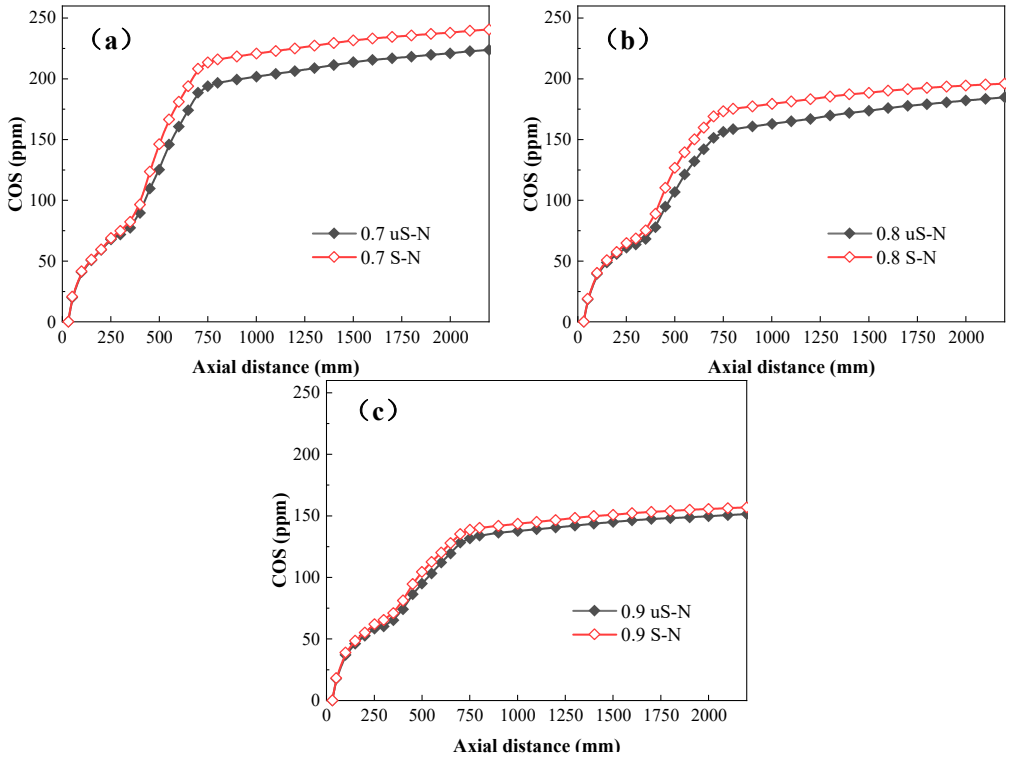

Figure 12. Effects of different excess air coefficients on COS concentration on the central axis of the coal combustion chamber for uS–N and S–N: (**a**) 0.7; (**b**) 0.8; (**c**) 0.9.

As shown in Figure 13, with an increase in the excess air factor, the concentration peak gap of CS_2 under the S–N condition and uS–N condition on the centreline of the furnace chamber keeps narrowing. At an excess air factor of 0.7, the contrast in peak CS_2 concentration between the S–N and uS–N conditions was 8.7%, which reduced to 8.0% at an excess air factor of 0.8, and further decreased to 6.9% at an excess air factor of 0.9. With an increase in the excess air factor, the difference in the decrease in the peak CS_2 concentration to the concentration at the furnace exit increased. The difference between the CS_2 generation rate at S–N operation and uS–N operation was 12.7% for an excess air factor of 0.7, 16.4% for an excess air factor of 0.8, and 21.1% for an excess air factor of 0.9. Such results could be attributed to the main combustion zone upstream of the furnace, with CS_2 generating SO radicals through the reactions of $CS_2 + O = CS + SO$ and $CS + O_2 = CO + SO$, and sulphur–nitrogen interactions consuming SO radicals through the reaction of $SO + NH = NO + SH$. The difference between the peak CS_2 concentration under S–N and uS–N conditions decreased with increasing excess air factor. In the reduction zone, CS_2 generated SH radicals through the reaction of $CS_2 + OH = COS + SH$. The sulphur–nitrogen interactions mainly promoted the consumption of CS_2 through the consumption of SH radicals through the reduction of NO. With an increase in the excess air coefficient, the production of NO also increased, leading to greater consumption of SH radicals and a subsequent decline in the amount of CS_2. With the increase in the excess air coefficient, the difference between the peak value of CS_2 concentration and the decrease in the concentration at the furnace outlet increased under the S–N condition and the uS–N condition. When the excess air factor is large, i.e., an excess air factor of 0.9 under fuel-rich conditions, the sulphur–nitrogen interactions should be included in the analysis of the corrosive sulphur-containing CS_2 gas.

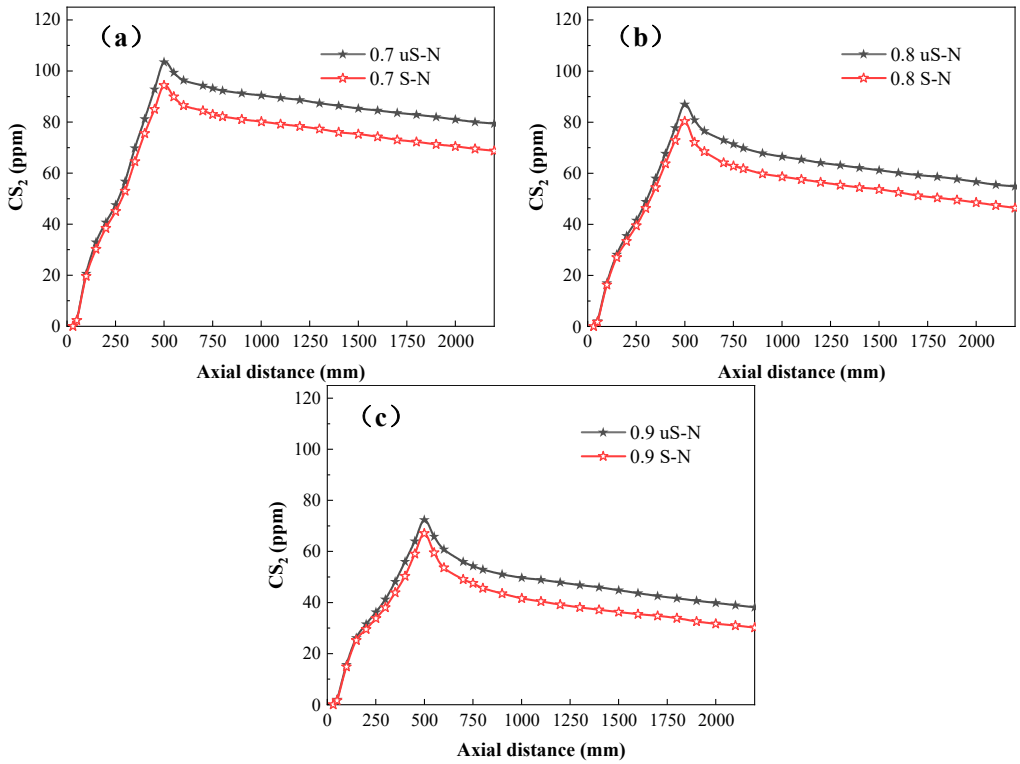

Figure 13. Effects of different excess air coefficients on CS_2 concentration on the central axis of the coal combustion chamber for uS–N and S–N: (**a**) 0.7; (**b**) 0.8; (**c**) 0.9.

4. Conclusions

In summary, a conventional sulphur component evolution model (uS–N) and an improved sulphur component evolution model (S–N), which considers sulphur–nitrogen interactions, were developed for the coal combustion process using OpenFOAM software, and the generation patterns of SO_2, H_2S, COS, and CS_2 were numerically calculated at different excess air coefficients. The results show the following:

(1) Compared with the uS–N working condition, the simulated values of sulphur components SO_2, H_2S, COS, and CS_2 under the S–N working condition were closer to the experimental values. Comparing the errors between the concentration values of sulphur components at the furnace outlet and the experimental values, the errors in the concentrations of SO_2, H_2S, COS, and CS_2 under S–N were 1.8%, 2.8%, 3.0%, and 4.1%, and the errors in the concentrations of each component were less than 5%; the error of SO_2 concentration when not considering the working conditions was 7.3%, whereas for the H_2S concentration, the error was 6.3%, the COS concentration was 9.0%, and the CS_2 concentration was 12.2%. A conclusion could be made that the S–N model was more precise in predicting the changes in sulphur components than the uS–N model.

(2) Within the simulation range, as the excess air factor increases, the production rate of SO_2 rises and the production rates of the corrosive sulphur components H_2S, COS, and CS_2 fall substantially. When the excess air coefficient is increased from 0.7 to 0.9, the production rate of SO_2 grows by 53.0%, while the production rates of H_2S, COS, and CS_2 drop by 41.3%, 34.8%, and 53.8%, respectively. Based on the simulation results, the excess air coefficient for the coal combustion process should be increased appropriately to reduce the production of corrosive sulphur-containing gases.

(3) The effects of the sulphur–nitrogen interactions on the generation rates of various components at different excess air coefficients were determined. When the excess air factor increases from 0.7 to 0.9, the difference between the SO_2 generation rates under S–N and uS–N conditions decreases from 13.4% to 3.5%. The difference in H_2S generation rates rises from 3.0% to 17.7%; the difference in COS generation rates falls from 7.6% to 4.0%;

and the difference in CS_2 generation rates grows from 12.7% to 21.1%. Furthermore, when the excess air factor is small, the effect of sulphur–nitrogen interactions on SO_2 and COS generation is more significant. In this case, the analysis of corrosive sulphur-containing COS gas should consider the sulphur–nitrogen interactions. Conversely, when the excess air factor is large, the effect of sulphur–nitrogen interactions on H_2S and CS_2 generation is more significant. Therefore, in this case, the analysis of corrosive sulphur-containing H_2S and CS_2 gases should include the sulphur–nitrogen interactions.

Author Contributions: Conceptualisation, Y.J., X.Y. and H.M.; methodology, Y.J., X.Y. and H.M.; software, Y.J., X.Y. and H.M.; writing—original draft preparation, Y.J., X.Y. and H.M.; writing—review and editing, Y.J., X.Y. and H.M. All authors have read and agreed to the published version of the manuscript.

Funding: This research was funded by the Fundamental Research Program of Shanxi Province (20210302123199) and the Major Special Projects of Science and Technology in Shanxi (20201102006).

Data Availability Statement: Data not available to be shared due to the technical limitations.

Conflicts of Interest: The authors declare no conflict of interest.

References

1. Zhou, Z.J.; Zhou, N.; Chen, Y.J.; Zhou, J.H.; Liu, J.Z.; Cen, K.F. Experimental research on the combustion and NO_X generation characteristics of low volatile coal. *Proc. CSEE* **2010**, *30*, 55–61.
2. Shirai, H.; Ikeda, M.; Aramaki, H. Characteristics of hydrogen sulfide formation in pulverized coal combustion. *Fuel* **2013**, *114*, 114–119. [CrossRef]
3. Maffei, T.; Sommariva, S.; Ranzi, E.; Faravelli, T. A predictive kinetic model of sulfur release from coal. *Fuel* **2012**, *91*, 213–223. [CrossRef]
4. Sugawara, K.; Tozuka, Y.; Sugawara, T.; Nishiyama, Y. Effect of heating rate and temperature on pyrolysis desulfurization of a bituminous coal. *Fuel Process. Technol.* **1994**, *37*, 73–85. [CrossRef]
5. Chen, C.; Horio, M.; Kojima, T. Numerical simulation of entrained flow coal gasifiers: Part I: Modeling of coal gasification in an entrained flow gasifier. *Chem. Eng. Sci.* **2000**, *55*, 3861–3874. [CrossRef]
6. Ströhle, J.; Chen, X.; Zorbach, I.; Epple, B. Validation of a detailed reaction mechanism for sulfur species in coal combustion. *Combust. Sci. Technol.* **2014**, *186*, 540–551. [CrossRef]
7. Von Bohnstein, M.; Yildiz, C.; Frigge, L.; Ströhle, J.; Epple, B. Simulation study of the formation of corrosive gases in coal combustion in an entrained flow reactor. *Energies* **2020**, *13*, 4523. [CrossRef]
8. Chagger, H.K.; Goddard, P.R.; Murdoch, P.; Williams, A. Effect of SO_2 on the reduction of NO_X by reburning with methane. *Fuel* **1991**, *70*, 1137–1142. [CrossRef]
9. Chagger, H.K.; Goddard, P.R.; Murdoch, P.L.; Williams, A. The interaction of SO_2 and NO in rich combustion zones. *Fuel* **1993**, *72*, 1451–1453. [CrossRef]
10. Choudhury, N.N.; Padak, B. An Investigation of the Interaction between NO_X and SO_X in Oxy-Combustion. *Environ. Sci. Technol.* **2017**, *51*, 12918–12924. [CrossRef]
11. Wang, X.; Si, J.; Tan, H.; Niu, Y.; Chen, E.; Xu, T. Interaction of SO_2 in a reduction-free process during methane re-combustion. *J. Eng. Thermophys.* **2011**, *32*, 4.
12. Wang, X.; Yablonsky, G.S.; Rahman, Z.; Yang, Z.; Du, P.; Tan, H.; Axelbaum, R.L. Assessment of sulfur trioxide formation due to enhanced interaction of nitrogen oxides and sulfur oxides in pressurized Oxy-combustion. *Fuel* **2021**, *290*, 119964. [CrossRef]
13. Xiao, H.; Zhou, J.; Liu, J.; Sun, B. Effect mechanism of existence patterns of sulphur on reduction of NO. *J. Fuel Chem. Technol.* **2008**, *36*, 381–384.
14. Kang, Z.; Feng, Z.; Sun, B. Chemical reaction kinetics analysis of H_2S generation in low NO_X combustion. *J. Combust. Sci. Technol.* **2022**, *28*, 652–658.
15. Yuan, L.Y.; Zhong, W.Q.; Chen, X.; Li, J.; Liu, G.Y.; Tian, W.J. Three-dimensional numerical simulation of variable load combustion of supercritical coal-fired boiler for deep peak load regulation. *JSEU* **2019**, *49*, 535–541.
16. Li, Z.; Zhang, Z.; Chen, D.; Cai, N.; Ran, Y.; Wang, J.; Zhang, D.; Wei, G.; Lin, S.; Zhou, W.; et al. Prediction of NO_X during pulverized coal combustion: Part 1—Model development and its implementation with Fluent. *J. China Coal Soc.* **2016**, *41*, 2426–2433.
17. Dagaut, P.; Glarborg, P.; Alzueta, M.U. The oxidation of hydrogen cyanide and related chemistry. *Prog. Energy Combust. Sci.* **2008**, *34*, 1–46. [CrossRef]
18. Wang, Z.; Zhou, H.; Zhou, J.; Pan, J.; Cen, K. Modeling and experimental study on NO_X reduction in furance with ammonia injection. *J. Fuel Chem. Technol.* **2004**, *32*, 48–53.
19. Soete, G. Overall reaction rates of NO and N2 formation from fuel nitrogen. *Symp. Int. Combust.* **1975**, *15*, 1093–1102. [CrossRef]
20. Luo, R.; Li, W.; Jiang, Y.; Bai, X. Distribution of sulfur in coals of China. *Coal Convers.* **2005**, *10*, 18–22.

21. Baruah, B.; Khare, P. Pyrolysis of high sulfur Indian coals. *Energy Fuels* **2007**, *21*, 3346–3352. [CrossRef]
22. Gu, Y.; Yperman, J.; Vandewijngaarden, J.; Reggers, G.; Carleer, R. Organic and inorganic sulphur compounds releases from high-pyrite coal pyrolysis in H_2, N_2 and CO_2: Test case Chinese LZ coal. *Fuel* **2017**, *202*, 494–502. [CrossRef]
23. Ma, H.; Zhou, L.; Ma, S.; Wang, Z.; Cui, Z.; Zhang, W.; Li, J. Reaction mechanism for sulfur species during pulverized coal combustion. *Energy Fuels* **2018**, *32*, 3958–3966. [CrossRef]
24. Liu, S.; Lv, S.; Hao, H.; Li, C.; Zhou, L.; Ma, H. Evaluation and simplification of detailed mechanism of sulfur species during pulverized coal combustion. *Clean Coal Technol.* **2021**, *27*, 139–148.
25. Lv, S.; Wang, B.; Zhao, J. A study on detailed mechanism of H_2S formation during pulverized coal combustion. *J. Xi'an Jiaotong Univ.* **2020**, *54*, 68–75.
26. Zhang, Z.; Cai, N.; Chen, D.; Imada, J.; Li, Z. Development of sulfur release and reaction model for computational fluid dynamics modeling in sub-bituminous coal combustion. *Energy Fuels* **2017**, *31*, 1383–1398. [CrossRef]
27. Clark, D.; Dowling, N.; Huang, M.; Svrcek, W.; Monnery, D. Mechanisms of CO and COS Formation in the Claus Furnace. *Ind. Eng. Chem. Res.* **2001**, *40*, 497–508. [CrossRef]
28. Abián, M.; Cebrián, M.; Millera, A.; Bilbao, R.; Alzueta, M. CS_2 and COS conversion under different combustion conditions. *Combust. Flame* **2015**, *162*, 2119–2127. [CrossRef]